

A microfluidic flow-converter based on a double-chamber planar micropump

Chia-Jui Hsu · Horn-Jiunn Sheen

Received: 26 June 2008 / Accepted: 14 August 2008 / Published online: 10 September 2008
© Springer-Verlag 2008

Abstract A microfluidic flow-converter that transforms an oscillatory flow into a steady-like flow in a reciprocating-type pumping device is successfully developed in this study. The flow quality at the outlet is found to be significantly improved. The present micro-device is composed of two single-chamber PZT micropumps in parallel arrangement and can be fabricated using simple micro-electromechanical-system (MEMS) techniques. Based on the concept of the electronic bridge converter, the flow rectification is supported by four passive planar valves. Two operation modes, in-phase and anti-phase, were used to test the performance of the present device. In addition, the flow characteristics at the outlet were examined by an externally triggered micro-PIV system. The results reveal that the current flow-converter provided both high volume and smoothly continuous flow rates at the outlet when it was in anti-phase mode. Moreover, the volume flow rate was linearly proportional to the excitation frequency within a specific frequency regime. This indicates that the flow-converter was easily operated and controlled. The present microfluidic flow-converter has great potential for integration into future portable micro- or bio-fluidic systems.

Keywords Flow-converter · Double-chamber micropump · Planar valve · Micro-PIV · Oscillatory flow

1 Introduction

Numerous researches on micropumps, which include developments and analyses, have been proposed in the past 30 years and widely introduced by the review papers. Based on the driving sources, a micropump can be classified as either a displacement type or a dynamic type (Laser and Santiago 2004). On the other hand, a micropump can also be called either a reciprocating type or a continuous flow type if the classification is made according to the flow behaviors (Woiias 2005). Recently, a more detailed classification of micropumps is also made according to the actuating principles and valve types (Iverson and Garimella 2008). The characteristics of various types of micropumps are compared and concluded in the review article. Most micropumps are developed based on the actuating principles of the reciprocating type micropump since it was first proposed in 1988 (van Lintel et al. 1988). A typical reciprocating micropump can be divided into two components: a chamber and two flow rectifiers.

The pumping chamber can be easily deformed by applying external driving sources such as PZT plates (Feng and Kim 2004), electromagnetic forces (Jeong and Yang 2000; Yamahata et al. 2005a, b), or thermopneumatic or pneumatic deformations (Sim et al. 2003; Huang et al. 2006). These forces vary within a time period due to the employment of AC driving signals, which lead to the pumping chambers have regular volume changes. Therefore, reciprocating flows exist in the microchannels.

The other component, flow rectifiers, which also plays an important role in directing flow can easily be classified as either valve type or valveless type. Rectifiers in a valve type can have high efficiency to block a reverse flow. Most valve-type rectifiers such as the cantilever valve (Zengerle et al. 1995; Koch et al. 1997; Loverich et al. 2007), ball valve

C.-J. Hsu · H.-J. Sheen (✉)
Institute of Applied Mechanics, National Taiwan University,
No. 1, Sec. 4, Roosevelt Road, Taipei 106, Taiwan, ROC
e-mail: sheenh@ntu.edu.tw

(Yamahata et al. 2005a, b; Pan et al. 2005), and planar floating valve (Papavasiliou et al. 1999) are actuated passive, which indicate that their motions mainly depend on the reciprocating flows. The valveless type rectifiers generate a net flow based on a direction-dependent resistance. Some examples, such as the nozzle/diffuser element (Gerlach et al. 1995; Gerlach and Wurmus 1995; Olsson et al. 2000; Hwang et al. 2008), the Tesla structure (Gamboa et al. 2006), and a combination form of nozzle/diffuser and Tesla structure (Izzo et al. 2007), show that the flow can be pumped out using these simple-patterned designs.

To summarize the results in the literatures, high pumping performances and simple fabrications are the essential design guidelines of earlier micropumps. In recent years, integrated micro-systems, called micro-TAS or lab-on-a-chip, have gained much attention, and more considerations are necessary when designing a novel micropump today. One of the considerations is how to integrate a micropump into a micro-system well. A complicated micropump design may perform high pumping performance but may not be able to combine with other elements. Simple micropump designs are always favorable for practical and commercial systems. Moreover, good pumping performance should be achieved based on low driving voltage requirements. Therefore, the efficiency for generating net flow per cycle must be raised. However, the results in our previous study (Sheen et al. 2008) have confirmed that the efficiency for generating net flow is low in an obstacle-type valveless micropump using a micro-Particle-Image-Velocimetry (micro-PIV) system.

One more thing that needs to be considered is the flow quality provided by the designed micropump. Oscillatory or pulsating flows can be expected in most reciprocating type micropumps. For example, the flow rectifier might completely block the reverse flow within a half-time period so that the flow pulsates at the outlet. This dramatic change of flow velocity may lead to some problems. For example, a flowmeter that monitors flow rates and forwards the signals to the control module might not, in practice, provide accurate results in determining flow velocities.

In this paper, a novel double-chamber planar micropump with simple patterns has been developed according to the guidelines mentioned above. The proposed micropump can be easily fabricated using the micro-electro-mechanical-system (MEMS) technique. Flows are driven by the PZT plates and are rectified by the planar passive valves. Pumping performances are tested using various excitation voltages as well as frequencies of the two operating modes: in-phase and anti-phase. To further investigate the characteristics of the micropump, flow fields are measured by a micro-PIV using externally triggered methods. Detailed procedures and results are presented in the following sections.

2 Experiments

2.1 Design and fabrication

Figure 1a and b, respectively show the photos of a micropump and a passive planar valve. Two circular pumping chambers of the same size, with diameters of 7 mm and a diaphragm thicknesses of 70 μm , are arranged in parallel. The length and width of the micropump are 25 and 20 mm, respectively. Two planar passive valves are placed, one upstream and one downstream, with each chamber directing flows during the pumping process. Each planar valve is composed of structures containing a moving part as well as obstacles with specific geometries in its channel. The T-shape moving part is confined by two rectangular blocks in order for it to have motion only along the axial direction. The dimensions of the moving part are labelled in Fig. 1b. The moving part has motion like a piston when it is driven by the oscillatory flow. The oscillatory flow is then rectified toward the outlet direction, i.e., from the left to the right direction in Fig. 1b. Moreover, the maximum displacement of the moving part is 70 μm , and this valve switches on and off depending on the directions of the oscillatory flows.

The PZT plates that adhered to the chambers provide periodical displacements, and the pumping processes for a single-chamber micropump can be divided into either a supply phase or a pump phase. At the supply phase, fluids are drawn from both the inlet and the outlet on to the chamber due to the decreasing pressure in the expanding-

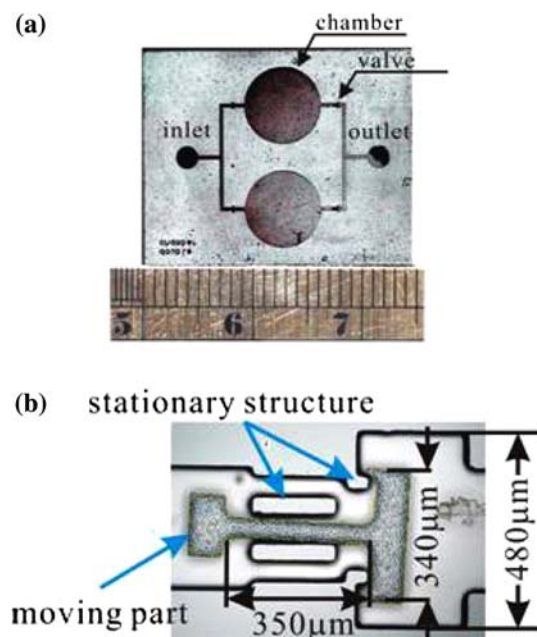


Fig. 1 Photos and dimensions of **a** double-chamber micropump, and **b** passive planar valve

volume chamber. During this, the upstream planar valve is opened while the downstream planar valve is closed. Therefore, the increase of fluid volume in the chamber is then mainly provided by the inlet. On the other hand, fluids are pumped out from the chamber due to the increasing pressure in the compressed volume at the pump phase. The pumped flow results in a switch-off and a switch-on of the upstream and downstream valves, respectively. Hence, the flow can only move toward the outlet, and thus, after an operating cycle, a net flow is obtained.

More factors need to be considered when two single-chamber micropumps work in parallel. Figure 2 illustrates the operating modes of the present double-chamber micropump, with in-phase and anti-phase modes. When a micropump is operated in in-phase mode, its two chambers are at supply and pump phases at the same time. On the other hand, a phase difference of 180° exists between the driving voltages for two PZT plates in anti-phase mode. The velocities of the oscillatory flows at the outlet are the sums of those pumped out from chambers A and B. Therefore, the oscillatory flow at the outlet is amplified when the micropump is operated in in-phase mode. Reduced amplitude, on the other hand, is obtained in the anti-phase mode, where a smoother flow rate is expected compared to the in-phase mode.

The fabrication process of the moving part and the device for the micropump is not complicated. Two single-polished silicon wafers $\langle 111 \rangle$, both with a thickness of $150 \mu\text{m}$, were used to fabricate the main device of the micropump and the moving parts of the valves. The silicon wafer for the manufacture of moving parts was etched in the first step in order to remove the superfluous thickness of $80 \mu\text{m}$. The thickness of the moving part was therefore

$70 \mu\text{m}$. An inductive couple plasma (ICP) etcher was employed to anisotropically etch the structures on the wafer. The photoresist, AZ-P4620, was then used to protect the patterns during the etching process and was removed by the O_2 plasma after the moving parts were released from the dummy wafer. The volume and mass of the moving parts are estimated to be $5.9 \times 10^{-3} \text{ mm}^3$ and $13.6 \mu\text{g}$, respectively. The process was used again to fabricate the main device of the micropump. The channels that connect the inlet and the outlet are $300 \mu\text{m}$ in width and $80 \mu\text{m}$ in depth. The silicon wafer was covered with a $500 \mu\text{m}$ thickness Pyrex 7740 glass plate with anodic bonding after the moving parts were manually placed in the channels. The PZT plates, with a diameter of 8 mm and thickness of $200 \mu\text{m}$, were attached to the silicon surface of the chamber with a thin layer of epoxy. The piezoelectric strain constants, d_{31} and d_{33} values of the PZT, were 190×10^{-12} and $420 \times 10^{-12} \text{ C/N}$, respectively. As shown in Fig. 1a, two holes were made at both the inlet and the outlet. Two glass tubes with an inner diameter of 1.15 mm were then connected, one to the inlet and the other to the outlet.

2.2 Measurements

Depleted ion water was served as the testing fluid to preliminarily measure the pumping performance of the experiment. A digital camcorder was used to record the variations of liquid levels in the glass tubes which were connected to the inlet and the outlet, respectively, in the vertical direction. The variations of the liquid levels were then evaluated to obtain the volume flow rates. Moreover, a micro-PIV system was employed to further investigate the transient flow fields within a time period for both in-phase and anti-phase modes. The principles are similar to traditional PIVs, but the illumination of the light sheet is replaced by other optical systems (Santiago et al. 1998). Flow motions were obtained by recording the displacements of the fluorescent particles seeded in the fluids. For most micro-PIV systems, the sampling rate, which ranges from several Hz to tens of Hz, is enough for steady flow measurements. Based on the Shannon-Nyquist theorem, this sampling rate cannot provide enough time resolution to analyze a high-frequency oscillatory flow motion with hundreds to thousands of Hz. Therefore, a micro-PIV measurement system with an externally triggered technique was used in our experiments. This technique has been previously employed to investigate unsteady flow fields in micromixers and microseparators (Sheen et al. 2007; Lee et al. 2007).

Figure 3 exhibits the schematic diagram of the instrumentation arrangement. The characteristics of phase-dependent flow fields were observed using a NikonTM

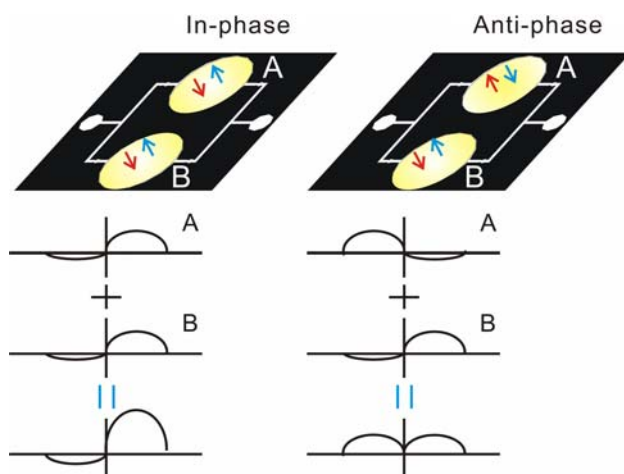
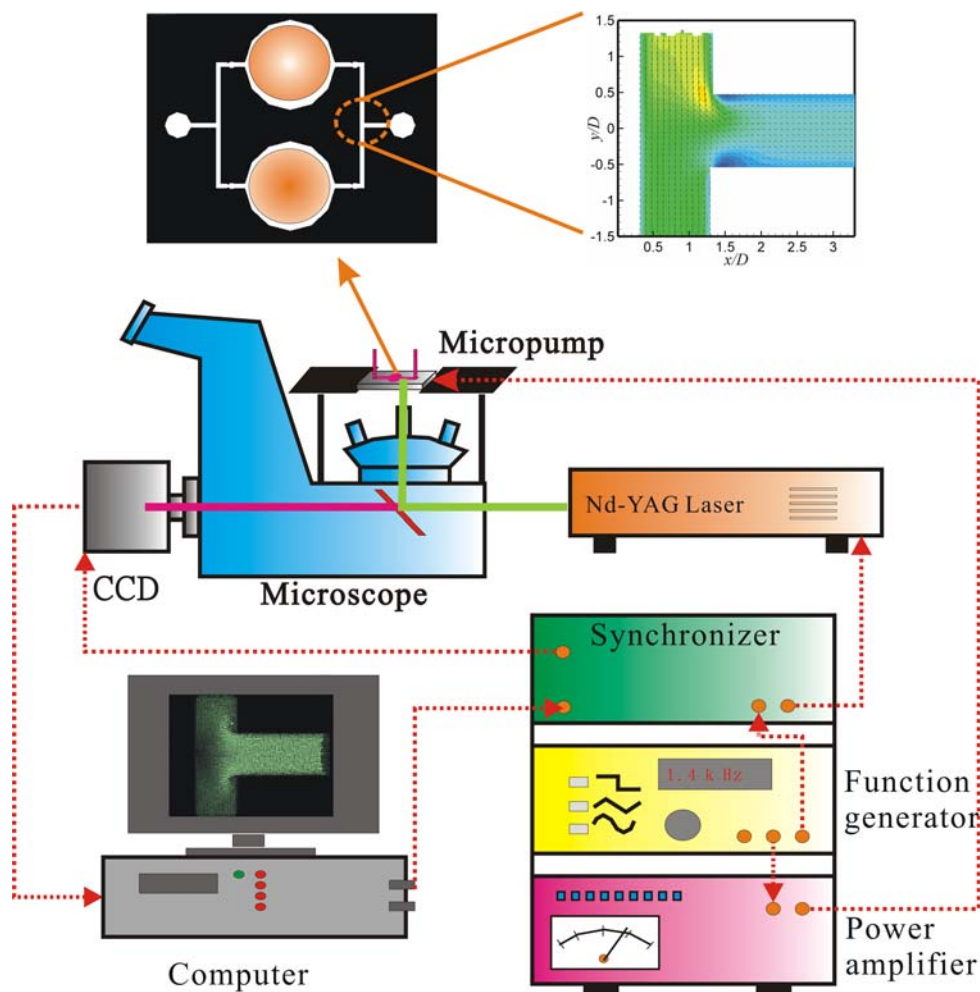


Fig. 2 Schematic diagram of the operating principles of a double-chamber micropump in the in-phase (left) and anti-phase (right) modes

Fig. 3 Instrumentation arrangement of an externally triggered micro-PIV system



inverted optical microscope. Fluorescent particles (Duke™) with 1 μm diameters were seeded in the depleted ion water with a volume ratio of less than 1%. The excitation and emission peaks of the particles were 542 and 612 nm, respectively. A double-pulsing Nd-YAG laser with a wavelength of 532 nm was used to illuminate the flow field. A liquid-light-guide was used to transmit and expand laser light to protect the optical system. A 10X object lens with a numerical aperture of 0.35 was used to collect fluorescent emissions. These emissions were then captured by a high-sensitivity CCD with a spatial resolution of $1,600 \times 1,200$ pixels.

The PZT plates were excited by the amplified square-wave signals, provided by a function generator and a power amplifier. The excitation voltages and frequencies of the square waves were 10–30 V (peak to peak) and 0.1–1.1 kHz, respectively. Externally triggered signals were also provided by the function generator, which kept the same reference time phases as its driving signals. A synchronizer was used as a timing and control module in this

experiment. Therefore, illumination, CCD exposure, and image capture were processed in a quick order whenever the synchronizer received externally triggered signals. The time resolution of the synchronizer is 10^{-9} s, which is much shorter than 0.01% of the cycling period. One hundred pairs of images (frame A and frame B) were captured and processed for each operating condition to eliminate the background noise. The flow fields were measured in the plane at the central depth and the velocities were evaluated by cross-correlation algorithm with Nyquist condition.

In our experiment, the interrogation window size chosen here was 16×16 pixels. That is the in-plane vector resolution was determined as $6.8 \times 6.8 \mu\text{m}$. The flow behaviours were analyzed at a time period of every 10 degrees. Based on the principle to reduced the Brownian errors, the choose of the time interval between frames A and B was varied from 5 to 200 μs . The shorter time interval was used for the higher flow velocities. Therefore, the Brownian error was thus controlled to be less than 1% for all results in a cycle.

Fig. 4 Volume flow rates in various operating modes at 10, 20, and 30 V (in-phase mode *filled diamond*, anti-phase mode *open diamond*, single-chamber A *filled circle*, and single-chamber B *open circle*)

3 Results and discussion

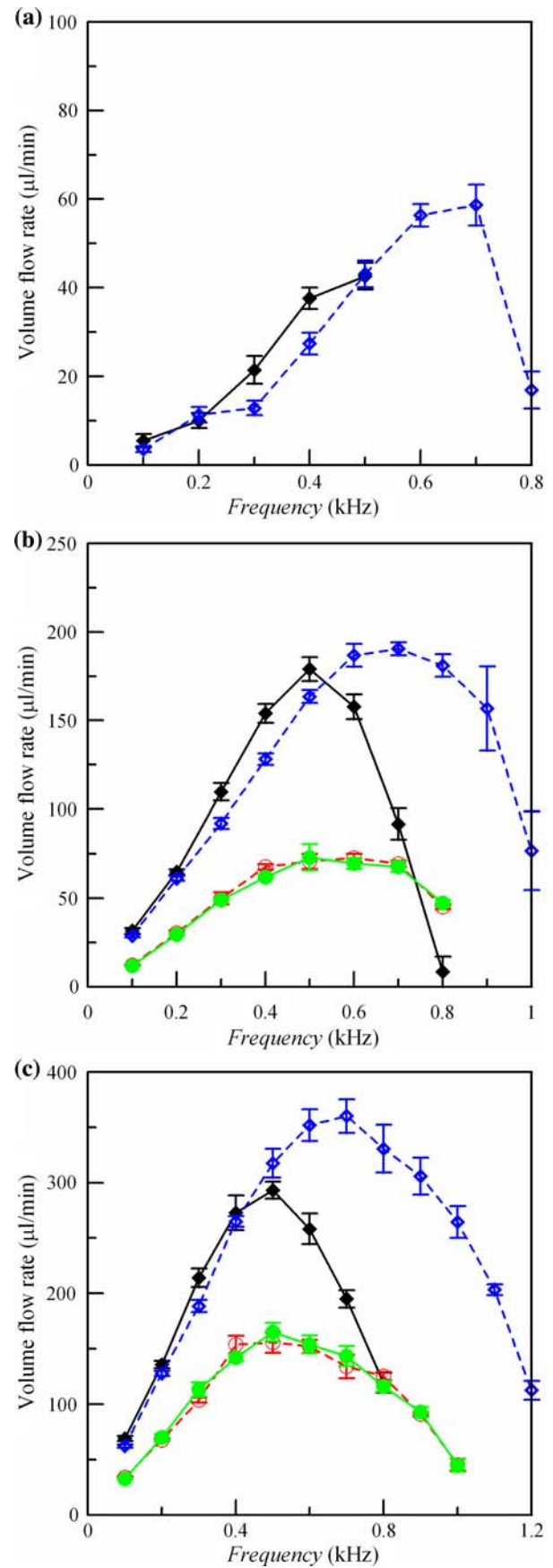
3.1 Pumping performance

Five different excitation voltages 10, 15, 20, 25, and 30 V were used to drive the PZT plates in both in-phase and anti-phase modes. Figure 4 reveals the pumping flow rates at 10, 20, and 30 V (the results for 15 and 25 V are not shown here). The black filled diamond and the blue open diamond symbols, respectively represent the flow rates measured in the in-phase and anti-phase modes. Moreover, the volume flow rates pumped by single chambers A (green filled circle) and B (red open circle) were also measured at the higher voltages of 20 and 30 V, as shown in Fig. 4b and c, respectively. The results clearly indicate that a wider range of frequencies were observed when the micropump was operated in the anti-phase mode than in the in-phase mode. The optimum frequencies of in-phase and anti-phase operations are at 0.5 and 0.7 kHz, respectively. The results also showed that the volume flow rates pumped by only one chamber, either A or B, were in good agreement with each other. In addition, Fig. 4b and c also indicate that the flow rates provided by single-chamber operations approximately amounted to half of those measured in the in-phase mode. The errors of the volume flow rates in the experiment were estimated according to the equation given as follows.

$$\frac{\delta \dot{Q}}{\dot{Q}} = \left[\left(2 \frac{\delta R}{R} \right)^2 + \left(\frac{\delta dh}{dh} \right)^2 + \left(\frac{\delta t}{t} \right)^2 \right]^{1/2} \quad (1)$$

where \dot{Q} , R , dh , and t are respectively the volume flow rate, the radius of the glass tube, the variation of the liquid level, and the time interval to record this variation. The measurement errors of these quantities are indicated by placing δ before the corresponding symbols. From the experiment, the errors of the measured volume flow rate were less than 8.5%.

Whether in in-phase or anti-phase mode, a linearly increasing flow rate with an increasing frequency was observed. For example, the linear regimes of in-phase and anti-phase mode operations were measured at 0.1–0.4 kHz and 0.1–0.5 kHz, respectively. These linear regimes made the present micropump easy to operate and control, which is very useful for a portable micro-TAS device. For example, a specific flow rate can be obtained by adjusting the excitation frequency to accord with the slopes of the linear relationships. Therefore, the flow of the testing sample for the sensing or mixing process in a micro biochemical system can be easily provided by the present



device. Furthermore, in order to verify how linear these relationships were, an index of linearity was determined by evaluating the correlation coefficient, ξ in the linear regimes. The definition of the correlation coefficient is given as follows:

$$\xi = \frac{\sum_{i=1}^n (x_i - \bar{x})(y_i - \bar{y})}{\sqrt{\sum_{i=1}^n (x_i - \bar{x})^2 \sum_{i=1}^n (y_i - \bar{y})^2}} \quad (2)$$

where x_i , y_i , \bar{x} , \bar{y} are the frequencies and the volume flow rates of the experimental results and the fitting lines, respectively. Here, n is the number of the testing data. Therefore, ξ will be 1 if a perfect linear relationship between variables x and y is found. The evaluations of the linearities in the linear regime for in-phase and anti-phase operations are listed in Table 1. The results clearly reveal that the values of ξ were higher than 0.99 in both operating modes whenever the excitation voltages went higher than 10 V. Lower correlation coefficients, which were still higher than 0.95, were obtained whenever a low driving voltage of 10 V was used in the tests. This low driving voltage and the reliable linear relationship between the flow rate and the frequency are favorable for the integration of the micropump into a micro-system.

3.2 Flowfield measurements using micro-PIV

Figures 5 and 6 illustrate the sequential flow fields within a time period T for in-phase and anti-phase modes, respectively. The measuring region includes the confluence connecting the channels to chambers A, B, and the outlet, all of which are marked in Fig. 3. Operating conditions were at 20 V and 0.5 kHz for both modes. The arrows represent the flow directions, while the contour colors indicate the magnitudes of the flow velocities. The red color represents a high velocity, while the blue means a lower one. Here, the normalized time $t/T = 0$ corresponds to the moment that the chamber volume starts to expand. These sequential flow fields clearly demonstrate how the flow moves within a time period. For example, the flows from chambers A (upper channel) and B (lower channel) were pumped out and drawn back at the same time in the in-phase mode as shown in Fig. 5. Therefore, the maximum flow velocity was measured in the channel connected to the outlet, and it does not matter whether this was done

at the pump or supply phases. Ideally, reversed flows are blocked by the passive valves, but the time for the valve to switch off can not, in practice, be neglected, so the leakage due to the reversed flow was measured. The results also indicate that the measured flow velocities from chambers A and B have slight differences, which might be due to the alignment errors of the PZT plates to the chamber diaphragms.

In anti-phase mode, the flow fields in Fig. 6 show that the flows pumping out or drawing back took place in turns between chambers A and B within a time period. An interesting phenomenon was observed in the sequential flow motions. During the time period from $-1/9$ to $3/9 T$, chamber A was at the supply phase while chamber B was at the pump phase. The lowest and the highest pressures thus respectively appeared in chambers A and B. Therefore, most of the flows that pumped out from chamber B went toward the upper channel until the valve downstream chamber A became completely closed. On the other hand, a small part of the flows then moved toward the outlet during the latter time phase. Opposite results were observed during time phases, from $4/9$ to $8/9 T$, so that the flow in the right channel was always toward the outlet within a time period.

Figures 7 and 8 reveal the phase-dependent flow velocities with respect to various frequencies in the in-phase and anti-phase modes. These velocities are the mean values which can be evaluated by integrating the velocity profiles along the horizontal sections according to the data given in Figs. 5 and 6. The red and blue lines represent the flows from chambers A and B, respectively, while the black line indicates the flow velocity at the outlet. In in-phase mode, Fig. 7a–d measured velocity variations within two operating cycles at 0.1, 0.3, 0.5, and 0.7 kHz, respectively. In the flows from chambers A and B to the right channel, the results show that the forward volume flow rates are much higher than the reversed flow rates when the micro-pump was operated at lower excitation frequencies such as 0.1 and 0.3 kHz. In addition, this clearly demonstrates that the flow in the right channel, i.e., the channel toward the outlet, equals the sum of the flows from chambers A and B. However, the reversed flow increases along with increasing frequencies, so that the pumping flow rates decreases at higher frequencies such as 0.5 and 0.7 kHz. When the excitation frequency goes higher than 0.7 kHz, the reversed flow rate becomes almost equal to the forward flow rate. This phenomenon leads to a net flow of zero.

In anti-phase modes, the phase-dependent flow rates within two cycles, measured at 0.1–1.1 kHz, are exhibited in Fig. 8a–f. The results show that the flow velocities at the outlet were much lower than those of chambers A and B. The reasons for these results are explained previously in

Table 1 Correlation coefficients in the linear regimes of the in-phase (0.1–0.4 kHz) and anti-phase (0.1–0.5 kHz) modes at various voltages

	10 V	15 V	20 V	25 V	30 V
$\xi_{\text{in-phase}}$	0.967	0.992	0.996	0.996	0.995
$\xi_{\text{anti-phase}}$	0.954	0.993	0.998	0.998	0.997

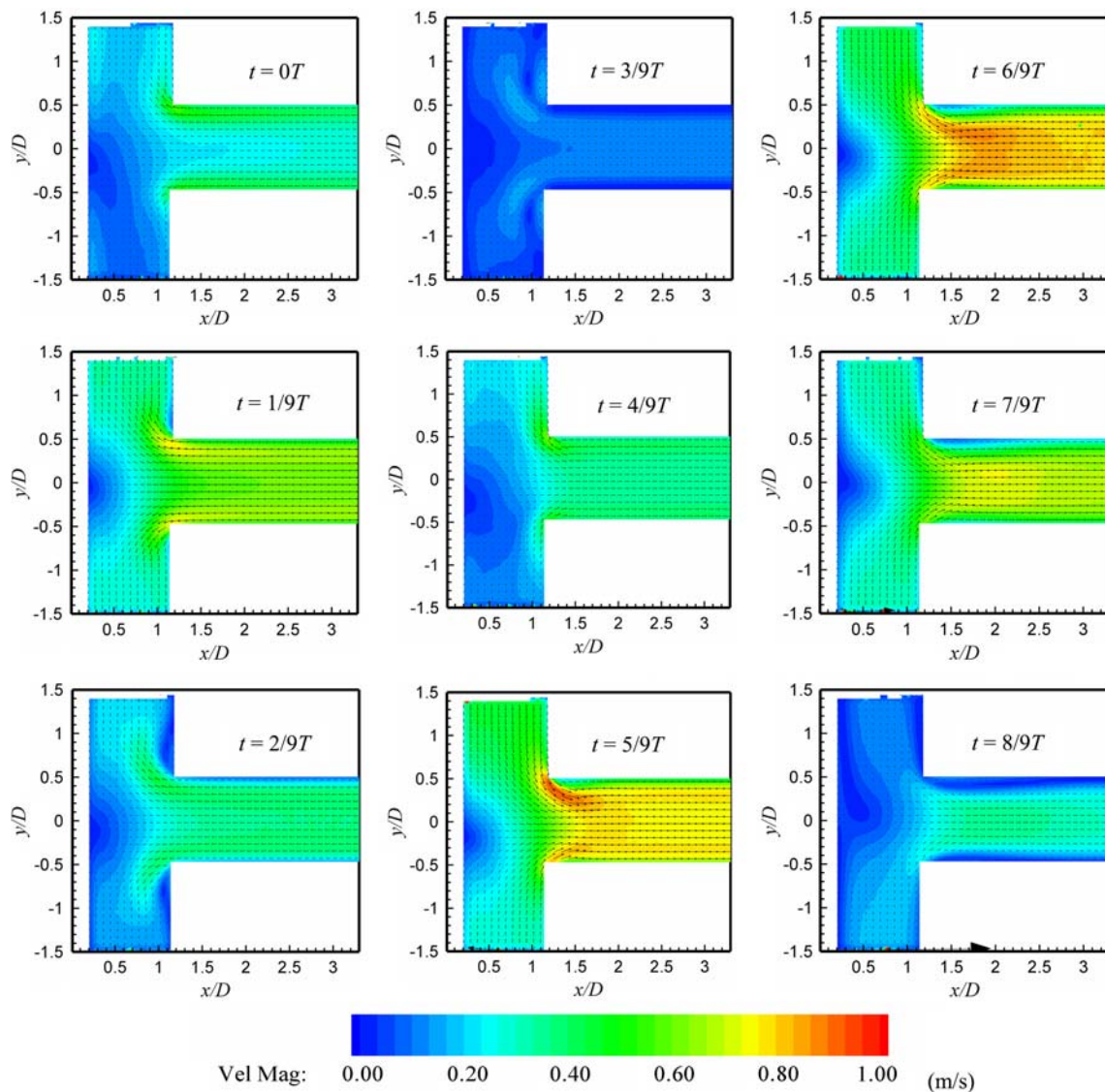


Fig. 5 Sequential flow fields in the in-phase mode within a time period. The voltage and frequency were measured at 20 V and 0.5 kHz, respectively

the discussion of Fig. 6. When one chamber pumped the flow toward the outlet, the other one performed a role of a capacitor to draw in most of the flows. Compared to the results in Fig. 7, the flow amplitudes at the outlet in the anti-phase mode were much lower than those in the in-phase mode. Moreover, two peaks of velocity amplitudes in a positive direction at the lower frequencies of 0.1–0.3 kHz were clearly observed within an operating cycle. This result indicated that the oscillatory flows from the two chambers were converted into a double-pulsating flow at the outlet. When higher excitation frequencies, from 0.5 to 0.9 kHz, were used to drive the micropump, the output flow became smoothly continuous. This result meant that the oscillatory flow always transformed into a steady-like flow toward the outlet at any given time. The flow moved

between chambers A and B whenever the frequency climbed higher than 1.0 kHz. Figure 8f depicts the output volume flow rate approaching 0 at 1.1 kHz.

In order to further quantify the performance of the current micropump according to the flow field measurement, the total flow diodicity of the two operation modes needed to be evaluated based on the determination, which is shown as follows:

$$\eta = 1 - \frac{Q_r}{Q_f} \tag{3}$$

where Q_f and Q_r are respectively the forward and reversed volume flows in the vertical central plane of the micro-channel. These volume flows are evaluated according to the integration of the phase-dependent velocities given in

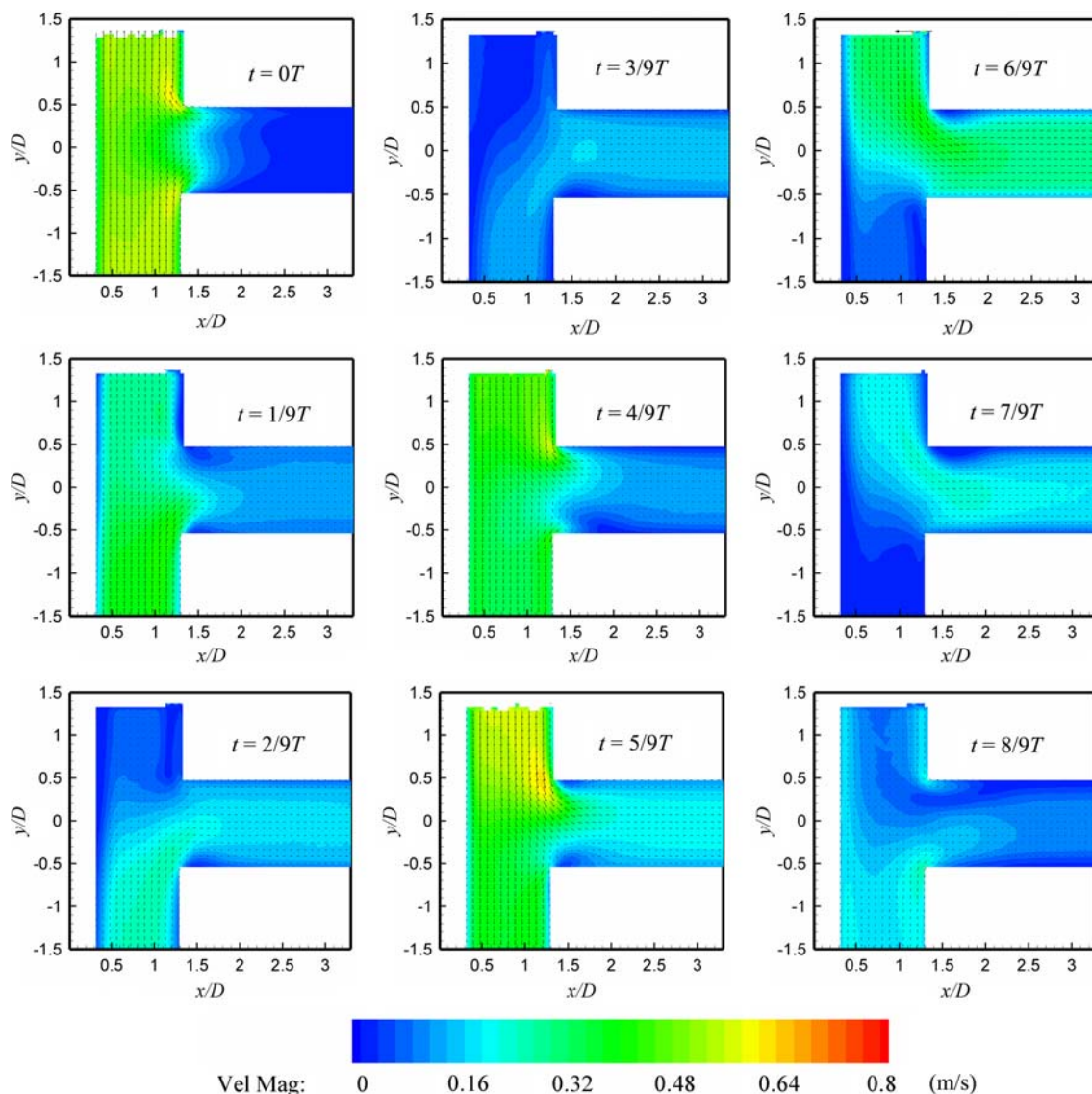


Fig. 6 Sequential flow fields in the anti-phase mode within a time period. The voltage and frequency were measured at 20 V and 0.5 kHz, respectively

Figs. 7 and 8. Although the volume flows were measured along the central plane, the volume flows in the other planes also revealed similar behaviors. Therefore, η can still be used as a typical index to estimate the total flow-rectifying capability. The value of η is 1 while there is no reversed flow and is 0 while $Q_r = Q_f$.

Figure 9 gives the values of η at various frequencies in the in-phase (black cross symbols) and the anti-phase (red diamond symbols) modes. In the in-phase mode, the value of η represents both the total flow-rectified capability as well as the net-flow generation efficiency. The results clearly indicate that η approximated a value of 0.5 in the in-phase mode at 0.1–0.5 kHz, and then decreased when the excitation frequency became higher than 0.5 kHz. On the other hand, it was found that η had a much higher value in

the anti-phase mode. In the frequency range from 0.1 to 1.0 kHz, η was higher than 0.8. The value came even close to 1 when it was at 0.6–1.0 kHz. Therefore, it can be concluded that the oscillatory flows from chambers A and B were successfully converted into a steady-like flow at the outlet. As the frequency went higher than 1.0 kHz, a rapid decrease of η was observed. The blue diamond symbols in Fig. 9 represent the flow conversion ratio, ψ , in the anti-phase mode. The determination for ψ is given as follows:

$$\psi = \frac{Q_f}{Q_A + Q_B} \quad (4)$$

where Q_A and Q_B are the volume flows pumped out from chambers A and B, respectively. The results clearly indicate that the net flows were about 40% of the sum of Q_A

Fig. 7 Phase-dependent velocities at **a** 0.1, **b** 0.3, **c** 0.5, and **d** 0.7 kHz provided by chamber A (red line), chamber B (blue line), and at the outlet (black line) during in-phase mode, with an excitation voltage of 20 V

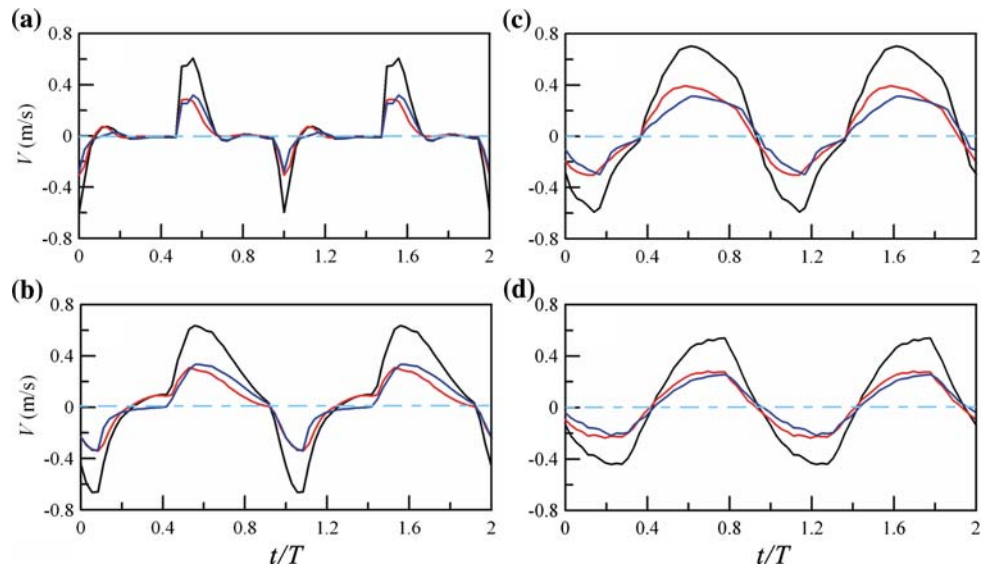
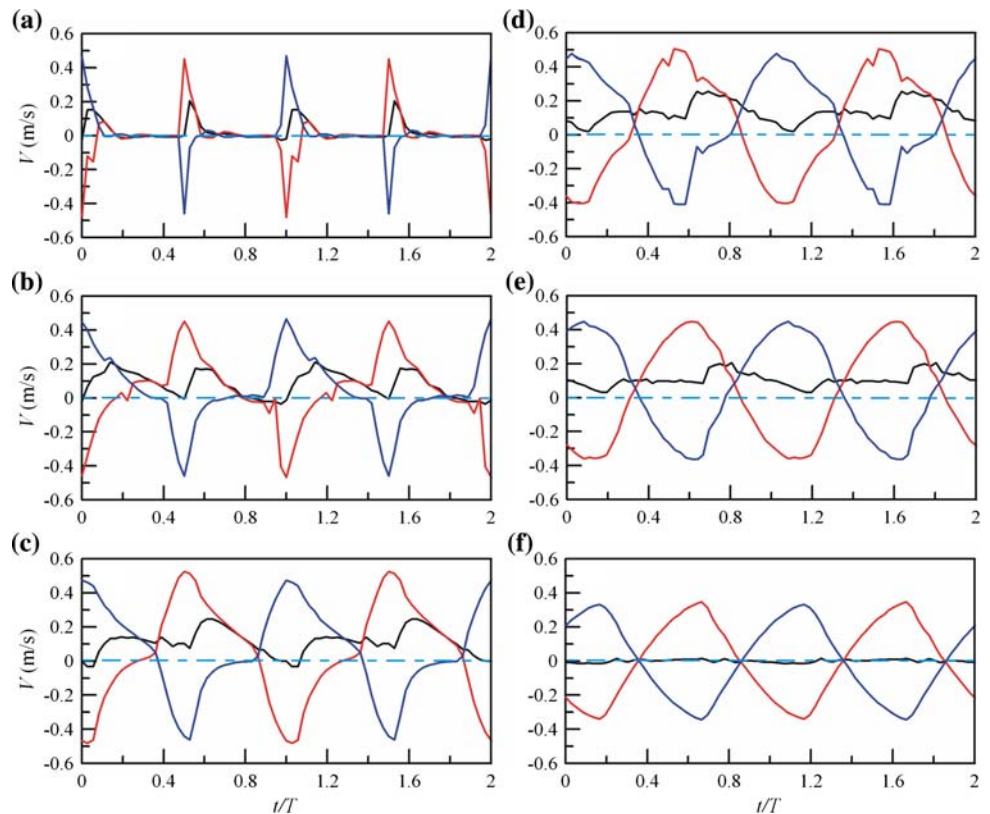


Fig. 8 Phase-dependent velocities at **a** 0.1, **b** 0.3, **c** 0.5, **d** 0.7, **e** 0.9, and **f** 1.1 kHz provided by chamber A (red line), chamber B (blue line), and at the outlet (black line) during anti-phase mode, with an excitation voltage of 20 V



and Q_B at 0.1–0.8 kHz. The 60% loss during the flow-converting process was mainly due to its capacitors, as mentioned in the previous paragraph. Moreover, the results also show that although the values of η still approximated 1 at 0.9 and 1.0 kHz, the value of ψ , however, rapidly decreased at frequencies higher than 0.8 kHz. The results measured at 0.1–0.5 kHz also show that the efficiency for generating the net flow in in-phase mode was 10% higher.

However, the total flow-rectified capability in anti-phase mode was almost twice that compared to in-phase mode.

4 Conclusions

In conclusion, a novel micro-device possessing both pumping and flow-converting capabilities was successfully

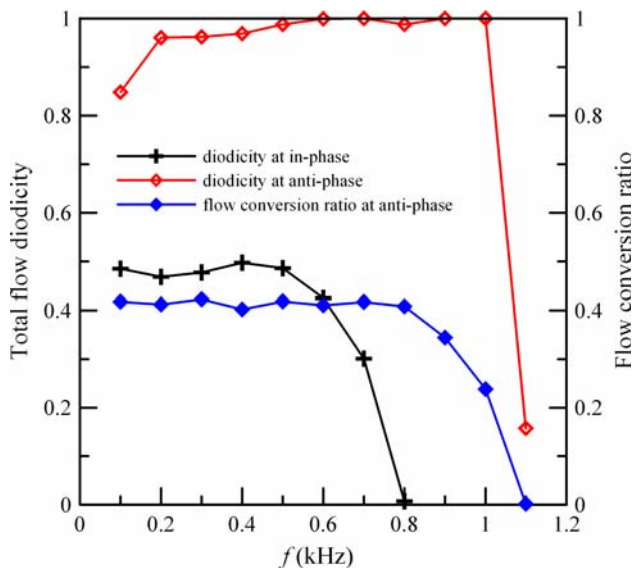


Fig. 9 Flow diodicities at various frequencies in the in-phase (*black marks*) and anti-phase modes (*red marks*). *Blue marks* represent the flow conversion ratios in the anti-phase mode

developed and tested in our study. The pumping performance of our present device uniquely provides reliable linear relationships between flow rates and excitation frequencies, which are very useful in a practical microsystem. The flow measurements using micro-PIV clearly demonstrated the process of how oscillatory flows were converted into a smoothly continuous flow in anti-phase mode operation. Based on flow rectifying capability and conversion ratio, the pumping performance and flow quality were found to possess optimal values when the operation frequencies were in the range of 0.2–0.8 kHz. In this frequency range, the value of η is higher than 0.9, and all conversion ratios approximate 0.4. In the future, the flow conversion ratio can be further raised by reducing the capacitor effect on the flow-converter. Therefore, a high-quality flow at the outlet of a reciprocating micropump, i.e., a nearly steady flow, can be effectively obtained by this microfluidic device.

Acknowledgments This work was supported by Ministry of Economic Affairs, 97-EC-17-A-05-A1-0017, and National Science Council, NSC 95-2218-E-002-051-MY3 of Taiwan, R.O.C.

References

Feng GH, Kim ES (2004) Micropump based on PZT unimorph and one-way parylene valves. *J Micromech Microeng* 14:429–435

Gamboa AR, Morris CJ, Forster FK (2006) Improvements in fixed-valve micropump performance through shape optimization of valves. *J Fluids Eng* 127:339–346

Gerlach T, Schuenemann M, Wurmus H (1995) *J Micromech Microeng* 5:199–201

Gerlach T, Wurmus H (1995) *Sens Actuators A* 50(1–2):135–140

Hwang IH, Lee SK, Shin SM, Lee YG, Lee JH (2008) Flow characterization of valveless micropump using driving equivalent moment: theory and experiments (in press). doi:10.1007/s10404-008-0275-7

Huang CW, Huang SB, Lee GB (2006) Pneumatic micropumps with serially connected actuation chambers. *J Micromech Microeng* 16:2265–2272

Iverson BD, Garimella SV (2008) Recent advances in microscale pumping technologies: a review and evaluation. *Microfluidics Nanofluidics* (in press). doi:10.1007/s10404-008-0266-8

Izzo I, Accoto D, Menciassi A, Schmitt L, Dario P (2007) Modeling and experimental validation of a piezoelectric micropump with novel no-moving-part valves. *Sens Actuators A* 133:128–140

Jeong OC, Yang SS (2000) Fabrication and test of a thermopneumatic micropump with a corrugated p+ diaphragm. *Sens Actuators A* 83:249–255

Koch M, Evans AGR, Brunnschweiler A (1997) Characterization of micromachined cantilever valves. *J Micromech Microeng* 7:221–223

Laser DJ, Santiago JG (2004) A review of micropumps. *J Micromech Microeng* 14:35–64

Lee CJ, Sheen HJ, Chu HC, Hsu CJ, Wu TH (2007) The development of a triple-channel separator for particle removal with self-pumping oscillating flow. *J Micromech Microeng* 17:439–446

Loverich J, Kanno I, Kotera H (2007) Single-step replicable microfluidic check valve for rectifying and sensing low Reynolds number flow. *Microfluidics Nanofluidics* 3:427–435

Olsson A, Stemme G, Stemme E (2000) Numerical and experimental studies of flat-walled diffuser elements for valve-less micropumps. *Sens Actuators A* 84:165–175

Pan T, McDonald SJ, Kai EM, Ziaie B (2005) A magnetically driven PDMS micropump with ball check-valves. *J Micromech Microeng* 15:1021–1026

Papavasiliou AP, Liepmann D, Pisano AP (1999) Fabrication of a free floating silicon gate valve. proceedings of the asme international mechanical engineering congress and exposition, Nashville, November 14–19, pp 435–440

Santiago JG, Wereley ST, Meinhart CD, Beebe DJ, Adrian RJ (1998) A particle image velocimetry system for microfluidics. *Exp Fluids* 25:316–319

Sheen HJ, Hsu CJ, Wu TH, Chang CC, Chu HC, Lei U (2007) Experimental study of flow characteristics and mixing performance in a PZT self-pumping micromixer. *Sens Actuators A* 139:237–244

Sheen HJ, Hsu CJ, Wu TH, Chang CC, Chu HC, Yang CY, Lei U (2008) Unsteady flow behaviors in an obstacle-type valveless micropump by micro-PIV. *Microfluidics Nanofluidics* 4:331–342

Sim WY, Yoon HJ, Jeong OC, Yang SS (2003) A phase-change type micropump with aluminum flap valves. *J Micromech Microeng* 13:286–294

van Lintel HTG, van de Pol FCM, Bouwstra S (1988) A piezoelectric micropump based on micromachining of silicon. *Sens Actuators* 15:153–167

Woiias P (2005) Micropumps—past, progress and future design. *Sens Actuators B* 105:28–38

Yamahata C, Lacharme F, Burri Y, Gijs MAM (2005a) A ball valve micropump in glass fabricated by powder blasting. *Sens Actuators B* 110:1–7

Yamahata C, Lotto C, Al-Assaf E, Gijs MAM (2005b) A PMMA valveless micropump using electromagnetic actuation. *Microfluidics Nanofluidics* 1:197–207

Zengerle R, Ulrich J, Kluge S, Richter M, Richete A (1995) A bidirectional silicon micropump. *Sens Actuators A* 50:80–86